Angewandte Chemie International Edition

Angewandte International Edition Chemie

GDCh German Chemical Society

How to cite: *Angew. Chem. Int. Ed.* **2026**, e8103353
doi.org/10.1002/anie.8103353

RESEARCH ARTICLE OPEN ACCESS Very Important Paper

An Artificial Molecular Pump Powered by Light

Federico Nicoli[1,2,3] | Chiara Taticchi[1,2] | Stefano Corra[1,2] | Marina Tranfić Bakić[1,2,4] | Massimo Baroncini[1,5] | Serena Silvi[1,6] | Jessica Groppi[1,7] | Alberto Credi[1,2]

[1]CLAN-Center for Light Activated Nanostructures, Alma Mater Studiorum – Università di Bologna and National Research Council of Italy (CNR), Bologna, Italy | [2]Dipartimento di Chimica Industriale "Toso Montanari", Alma Mater Studiorum – Università di Bologna, Bologna, Italy | [3]Institut de Science et d'Ingénierie Supramoléculaires (ISIS), University of Strasbourg & CNRS UMR 7006 8 Allée Gaspard Monge, Strasbourg, France | [4]Faculty of Chemistry and Technology, University of Split Ruđera Boškovića, Split, Croatia | [5]Dipartimento di Scienze e Tecnologie Agro-alimentari, Alma Mater Studiorum–Università di Bologna, Bologna, Italy | [6]Dipartimento di Chimica "G. Ciamician", Alma Mater Studiorum–Università di Bologna, Bologna, Italy | [7]Institute for Organic Synthesis and Photoreactivity (ISOF), National Research Council of Italy (CNR), Bologna, Italy

Correspondence: Jessica Groppi (jessica.groppi@cnr.it) | Alberto Credi (alberto.credi@unibo.it)

Received: 23 January 2026 | **Revised:** 16 March 2026 | **Accepted:** 26 March 2026

Keywords: azobenzene | molecular motor | photochemistry | rotaxane | supramolecular chemistry

ABSTRACT

Replicating the ability of biological systems to convert energy into directional molecular motion to perform functions is a central challenge in nanoscience. Artificial molecular pumps that can move substrates energetically uphill remain elusive, particularly when powered by light in an autonomous fashion. We report a molecular pump that uses light to actively transfer macrocycles from solution into a high-energy intramolecular compartment. The system operates via a photon-driven energy ratchet mechanism, sustaining a non-equilibrium distribution of species under continuous irradiation. All relevant kinetic and thermodynamic parameters were determined, and a comprehensive mechanistic model was developed. This minimalistic and robust design establishes a foundation for fully synthetic light-controlled non-equilibrium systems with potential applications in adaptive materials and solar energy conversion.

1 | Introduction

Living organisms rely on sophisticated molecular systems that convert external energy inputs into functions, such as transport, regulation and replication, by means of controlled molecular movements [1]. These nanoscale motors operate away from chemical equilibrium by continuously dissipating energy and performing controlled movements of their molecular components and substrates [2]. Among such systems, ion pumps—namely, biomolecular motors that can use an energy supply to move ions directionally in the absence of a chemical gradient, or against it—are widespread and play a crucial role for life [3].

Since the advent of artificial molecular machines [4], there has been considerable interest in the development of synthetic systems that can move molecules [5–7] or ions [7–9] energetically uphill [10–13]. As the field progressed [14], and the underlying fundamental principles became better understood [15–18], prototypes of artificial molecular pumps began to be reported [19]. In recent years, promising examples driven by chemical [20, 21] and electrochemical [22] energy were described. However, the rational development of synthetic molecular pumps that can process energy autonomously and operate away from equilibrium remains extremely demanding [14–19].

Federico Nicoli and Chiara Taticchi contributed equally to this work.

In memory of Professor Fraser Stoddart.

In this context, making molecular pumps capable of harnessing light energy in the form of visible or near-UV photons would be a far-reaching goal for both basic science and technological purposes. Light excitation can provide excellent spatiotemporal and intensity control, induce clean and reversible transformations, avoid the formation of waste products, and represent a non-invasive tool, also for biological matter [23]. It is worth noting that the direct conversion of light energy into molecular motion is a rare event in nature, the only notable exception being the bacteriorhodopsin proton pump [24]; in most instances, the energy is first converted by photosynthesis into an electrochemical potential, which is ultimately employed to produce chemicals (e.g., adenosine triphosphate) that power biomolecular motors [25]. This blueprint was followed in early outstanding reports of hybrid (natural-artificial) transmembrane ion pumps [26, 27]. Nonetheless, the opportunities offered by supramolecular photochemistry [23, 28] make it possible to rationally design synthetic systems that can directly convert light into directional molecular movements [29–33] and store the energy in non-equilibrium states [34–37] or enable the synthesis of thermodynamically unfavored molecular structures [38, 39]. In perspective, novel and unconventional approaches for artificial photosynthesis [40] could emerge.

Despite promising preliminary studies [41–43], artificial molecular pumps powered by light that translate their operation into a tangible effect are still missing. Recently, light-driven transport of ions or molecules across phase-separated compartments was demonstrated [44, 45], in these cases, however, the function relies on macroscopic asymmetry (most typically, differential irradiation at the two arms of a U-tube) rather than on molecularly engineered properties.

In our laboratory we described [46], optimized [47–49] and thoroughly characterized [50, 51] a supramolecular rotaxane-type assembly in which light irradiation causes the directionally biased transit of a macrocycle relatively to a non-symmetric (oriented) axle owing to a photon-driven energy ratchet mechanism. The system is modular, robust and simple, and it can autonomously harness light energy to create non-equilibrium concentrations of the species involved; until now; however, it has operated in solution, where the lack of organization prevents the pumping effect from being used to accumulate chemical potential. Here we report on a device that exploits the light-driven process described above to capture macrocycles from solution and move them energetically uphill along the thread, thus behaving as a photochemically driven molecular pump.

2 | Results and Discussion

2.1 | Design and Operation of the Pump

The photoactive component of the device, *E*-**1** (Figure 1a) consists of two main compartments: (i) a light-driven pumping module and (ii) a ring collecting thread, or reservoir. The former comprises an azobenzene photoswitch—the light-powered engine—linked to a benzylammonium recognition site (pumping station, I), and the latter is a C_{10} alkyl chain terminated with a dibenzylammonium recognition site (receiving station, II) equipped with bulky t-Bu substituents to prevent macrocycle dethreading on that side. The macrocycle **2** (Figure 1a) is a dibenzo-24-crown-8 (DB24C8) ether labelled with a trifluoromethyl (—CF_3) group that allows the ring to be monitored by ^{19}F nuclear magnetic resonance (NMR) spectroscopy.

Figure 2 shows the reaction network and potential energy diagrams that represent the planned operation of the pump. Mixing *E*-**1** and **2** in the dark results in the initial formation of the complex on station I, *E*-**1**⊂**2**^{I}, by fast threading of one macrocycle onto the *E*-azobenzene (Figure 2a). Shuttling of **2** between the two ammonium stations on **1** enables the interconversion between the two co-conformations of the [2]pseudorotaxane, namely *E*-**1**⊂**2**^{I} and *E*-**1**⊂**2**^{II}, which differ solely for the position of the ring, either on station I or II. Then, a second crown ether can be complexed to form a [3]pseudorotaxane, *E*-**1**⊂(**2**)$_2$, in which both stations are encircled by a ring. The distribution of free and complexed species at equilibrium in the dark is governed by the binding constants of the I and II stations with **2**. Under light irradiation, the *E*-azobenzene unit is transformed into the *Z*-isomer (Figure 1b), and the corresponding complexes *Z*-**1**⊂**2**^{I}, *Z*-**1**⊂**2**^{II}, and *Z*-**1**⊂(**2**)$_2$ are obtained. As previously demonstrated [46, 48–50], azobenzene photoisomerization has two main consequences: (i) an increase of the energy barrier for ring threading, and (ii) a decrease of the binding constant with the neighboring ammonium station. These phenomena make up the energy ratchet mechanism that determines the directional transit of the ring along the axle. However, while in the pump model the macrocycles are up-taken from and released into the same solution, in the current system we envisioned that the crown ether expelled from station I would move toward the collecting compartment, thereby increasing the ring population on station II beyond its equilibrium value (Figure 2b). Since the same photons can trigger both *E*→*Z* and *Z*→*E* isomerization, it can be expected that continuous light irradiation brings the system into a dissipative regime in which it can autonomously collect rings from solution and trap them intramolecularly in a high energy state.

2.2 | Spectroscopic and Photochemical Characterization

Upon dissolving an equimolar amount of *E*-**1** and **2** in CD_2Cl_2/CD_3CN 3:7, signals associated with the formation of pseudorotaxanes, in which both ammonium sites on the axle are encircled by the macrocycle, are detected by ^{1}H and ^{19}F NMR spectroscopy (Figure 3 and Supporting Information, section 3.2). Specifically, the ^{1}H NMR peaks of the benzylic protons adjacent to the ammonium stations in **1** (Figure 3a, blue and cyan), undergo deshielding and present the characteristic pattern of threaded DB24C8-dialkylammonium complexes [47]. As the complexation equilibria are slow on the NMR timescale, two sets of signals can be identified in the dark besides the peaks of the free species: One attributable to the complexed station I (Figure 3c, blue), and one related to the complexed station II (Figure 3c, cyan). Analogously, the ^{19}F NMR spectra show that the resonance of the —CF_3 group on the macrocycle (Figure 3b) evolves into two distinct singlets, corresponding to the ring located either on I or II (Figure 3d, marked respectively in blue and cyan). Irradiation of the solution at $\lambda = 365 \pm 5$ nm causes *E*→*Z* isomerization of the azobenzene group, leading to the emergence of a new set of signals assigned to the complexed station I in the *Z*-isomer (Figure 3ef, orange).

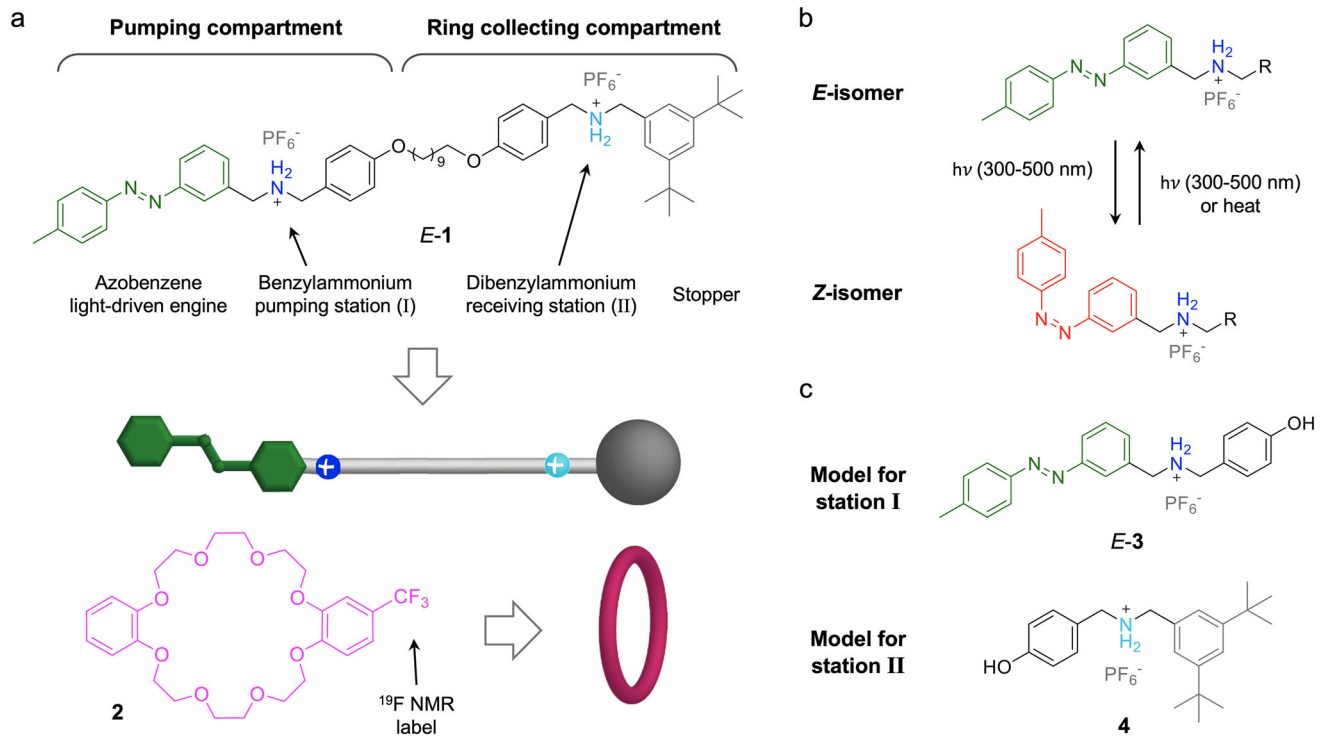

FIGURE 1 | Chemical structure and functional elements of the investigated system. (a) Molecular formula and cartoon representation of the pump components, axle *E*-**1** and macrocycle **2**. (b) The reversible isomerization of the azobenzene unit of the investigated compounds between *E*- and *Z*-configurations. (c) Molecular formula of model compounds *E*-**3** and **4**.

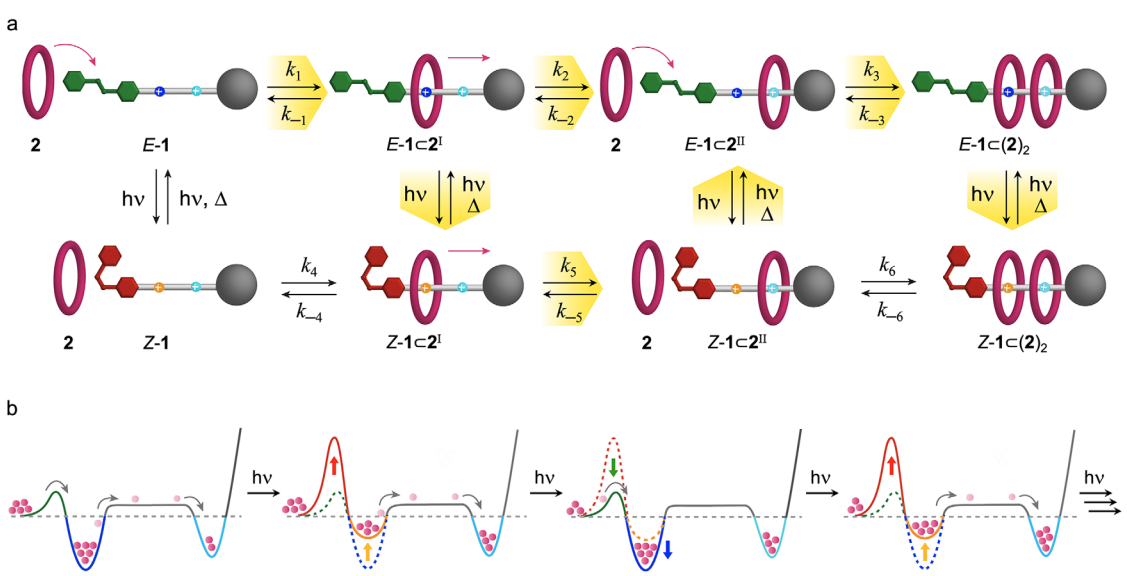

FIGURE 2 | Reaction scheme and operating principle of the molecular pump. (a) The network of reactions that describes the operation of the molecular pump; please refer to Figure 1a for description of the cartoons. The complexation equilibria and isomerization reactions are the horizontal and vertical processes, respectively; light is involved only in the vertical processes. k_n are the rate constants of the corresponding reactions, while the subscripts hν and Δ denote the photochemical and thermal isomerization processes, respectively. The pink arrows and yellow background highlight respectively the ring steps and reactions that are functional to pumping. A complete scheme with the description of all reaction parameters is reported in the Figure S55. (b) Simplified energetic profiles (potential energy versus ring-axle relative position) that describe the light-driven energy ratchet at the basis of pumping. The number of pink disks represents the ring population in the various states: uncomplexed, complexed at station I, and complexed at station II. Overall, repeated $E \leftrightarrows Z$ isomerization by continuous light irradiation results in the accumulation of the [3]pseudorotaxane and in the depletion of the free macrocycle.

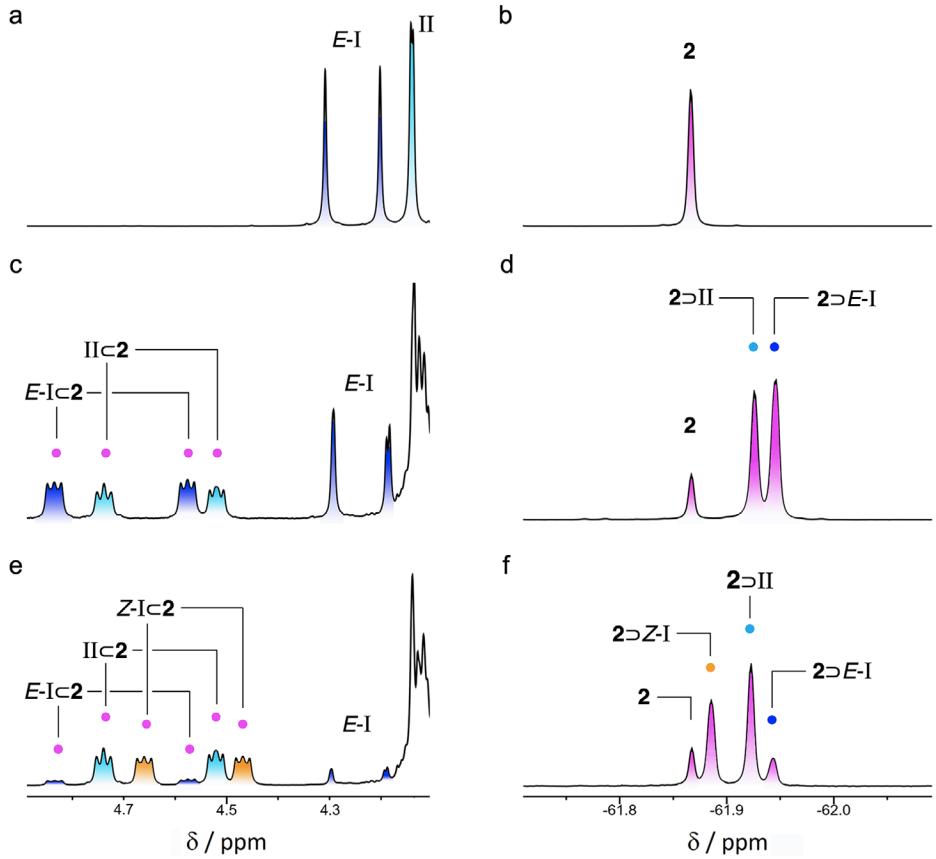

FIGURE 3 | Partial NMR spectra (CD_2Cl_2/CD_3CN 3:7, 298 K) showing the changes in the peaks associated with the —CH_2—NH_2^+—CH_2— moiety of axle **1** (a, c, e; ^{1}H NMR) and the —CF_3 group of ring **2** (b, d, f; ^{19}F NMR). (a) ^{1}H NMR spectrum of *E*-**1** (10 mM, 500 MHz). (b) ^{19}F NMR spectrum of **2** (10 mM, 470 MHz). (c) ^{1}H NMR (10 mM, 500 MHz) and (d) ^{19}F NMR (10 mM, 470 MHz) spectra of an equilibrated 1:1 mixture of *E*-**1** and **2**. (e) ^{1}H NMR (10 mM, 500 MHz) and (f) ^{19}F NMR (10 mM, 470 MHz) of an equilibrated 1:1 mixture of *E*-**1** and **2** after exhaustive irradiation at $\lambda = 365$ nm. The signals of the stations in a, c, and e are color-coded and those corresponding to stations encircled by a macrocycle are marked with a magenta dot. In (d) and (f), each coloured dot on a particular signal identifies the station encircled by the ring. The colours are coherent with those of the cartoons in Figure 2a, namely: blue, station *E*-I; orange, station *Z*-I; cyan, station II; magenta, ring **2**. Given the impossibility to deconvolute the signals of the individual compounds, each label in the graph (except **2**) refers to all the species that have the same azobenzene configuration and/or station occupancy. Hence, the signals labelled *E*-I are the convolution of the resonances of the species that possess an *E*-azobenzene unit and an uncomplexed station I, namely *E*-**1** and *E*-**1**⊂**2**^{II}; similarly, II = *E*-**1** + *E*-**1**⊂**2**^{I} + *Z*-**1** + *Z*-**1**⊂**2**^{I}; *E*-I⊂**2** (or **2**⊃*E*-I) = *E*-**1**⊂**2**^{I} + *E*-**1**⊂(**2**)$_2$; *Z*-I⊂**2** (or **2**⊃*Z*-I) = *Z*-**1**⊂**2**^{I} + *Z*-**1**⊂(**2**)$_2$. II⊂**2** (or **2**⊃II) = *E*-**1**⊂**2**^{II} + *E*-**1**⊂(**2**)$_2$ + *Z*-**1**⊂**2**^{II} + *Z*-**1**⊂(**2**)$_2$. See the text for details.

While isomerization induces a significant shift ($\Delta\delta \cong 0.15$ ppm) of the ^{1}H NMR signals associated with station I, in line with earlier observations [46, 48, 49], the peaks related to II are unaffected, suggesting that the receiving station is far enough away from the pumping compartment that it is not affected by it.

It should be remarked that both [2]pseudorotaxane co-conformations, where the ring encircles either I or II, and the [3]pseudorotaxanes, characterized by rings on both stations, are formed as depicted in the reaction scheme in Figure 2a and confirmed by mass spectrometry (Figures S41 and S43–S45). Unfortunately, the diagnostic NMR resonances of the [3]pseudorotaxane species are isochronous to those of the [2]pseudorotaxanes, preventing the monitoring of their variations separately. This observation, together with the perfect correspondence between the binding constants of stations I and II in *E*-**1** and in the related model compounds (Supporting Information, section 3.3), strongly suggests that the two stations behave independently of each other, and any (anti)cooperative effect can be ruled out.

The UV–vis absorption spectra of axle **1** and its complexes with **2** are in line with those of previously studied related systems (Supporting Information, section 4). The *Z*-isomer fraction at the photo stationary state (PSS) reached upon irradiation at 365 nm in CH_2Cl_2/CH_3CN 3:7 is 97% for **1** alone and 95% in the presence of a large excess of **2**. The *Z*→*E* back-isomerization can be triggered either photochemically or thermally; in both cases, the free and complexed axle behave the same—for example, similar PSS compositions upon irradiation at 436 nm and dark isomerization rate constants ($k_{Z\rightarrow E,\Delta} \cong 10^{-6}$ s^{-1}).

2.3 | Thermodynamic and Kinetic Parameters

The complexity of the mixture, further enhanced by irradiation, prevents the deconvolution of the contribution of each species to the NMR and UV-vis spectral changes. The binding constants of the macrocycle with either ammonium recognition site of the axle were estimated from ^{1}H NMR experiments on **2** in the presence of either *E*-**3**, *Z*-**3**, or **4** (Figure 1c), which are models

TABLE 1 | Rate constants and activation free energies of the thermal reactions.[a]

	k_1 (k_3)[b] (M^{-1} s^{-1})	$\Delta G^{\ddagger}_1$[c] (kJ mol–^{1})	k_{-1} (k_{-3})[d] (s^{-1})	$\Delta G^{\ddagger}_{-1}$[c] (kJ mol–^{1})	k_2[e] (s^{-1})	$\Delta G^{\ddagger}_2$[c] (kJ mol^{-1})	k_{-2}[e] (s^{-1})	$\Delta G^{\ddagger}_{-2}$[c] (kJ mol^{-1})
E-**1** + **2**	19	66	1.8×10^{-2}	83	3.2×10^{-3}	87	5.2×10^{-3}	86
	k_4 (k_6)[e] (M^{-1} s^{-1})	$\Delta G^{\ddagger}_4$[c] (kJ mol^{-1})	k_{-4} (k_{-6})[f] (s^{-1})	$\Delta G^{\ddagger}_{-4}$[c] (kJ mol^{-1})	k_5[g] (s^{-1})	$\Delta G^{\ddagger}_5$[c] (kJ mol^{-1})	k_{-5}[e] (s^{-1})	$\Delta G^{\ddagger}_{-5}$[c] (kJ mol^{-1})
Z-**1** + **2**	1.1×10^{-3}	90	1.8×10^{-6}	106	5.6×10^{-3}	86	5.2×10^{-3}	86

[a] CD_2Cl_2/CD_3CN 3:7, 298 K.

[b] Determined by stopped flow UV–vis absorption technique.

[c] Activation free energies calculated with the equation $\Delta G^{\ddagger} = -RT \ln(kh/k_B T)$, where R is the gas constant, h is the Planck constant, and k_B is the Boltzmann constant.

[d] Calculated as $k_{-1} = k_1/K_{E\text{-I}}$.

[e] Determined by time resolved ^{1}H NMR spectroscopy.

[f] Calculated as $k_{-4} = k_4/K_{Z\text{-I}}$.

[g] Calculated according to the set of equations reported in the Supporting Information, section 6.2.

for the portions of **1** containing the pumping station (I) near *E*- or *Z*-azobenzene, and the receiving station (II), respectively (Supporting Information, section 3.3 and Table S1). The data highlight the destabilization of the complex at station I caused by *E*→*Z* isomerization: the binding constant of the pumping station decreases from $K_{E\text{-I}}$ = 1030 ± 60 M^{-1} to $K_{Z\text{-I}}$ = 590 ± 60 M^{-1} ($K_{E\text{-I}}/K_{Z\text{-I}}$ = 1.7, $\Delta\Delta G°$ = 1.4 kJ mol^{-1}), thereby confirming the possibility to generate a dissipative non-equilibrium state. The higher affinity of **2** for station *E*-I can be explained by considering the inductive effect of the electron-withdrawing azo group that increases the acidity of the adjacent benzylammonium site. The binding constant of the receiving station is K_{II} = 650 ± 20 M^{-1}; therefore, the overall ring affinity trend is *E*-I > II ≳ *Z*-I.

The kinetic constants associated with thermal reactions in the network (Figure 2a) were determined by a combination of UV–vis and NMR spectroscopies (Table 1). Threading of **2** on the *E*-azobenzene extremity of **1** was monitored by stopped-flow UV–vis spectroscopy; the rate constant k_1 is coherent with previous experiments on the pumping module (Figure S54). An equilibration process follows, involving shuttling of **2** from station I to II, which was monitored by ^{1}H NMR. In agreement with the binding constants determined for the model compounds, at equilibrium the ensemble of species with a complexed station *E*-I is more populated than that of the species with a complexed station II (Figure 3c,d). Rate constants k_2 and k_{-2} were determined by fitting the time dependent concentration profiles, extracted from ^{1}H NMR data, with a mixed-order kinetic model (Figure S52). In consequence of the high affinity of the ring for stations I and II, shuttling along the collecting chain is quite slow ($t_{1/2}$ of ring transfer from I to II is about 4 min at 298 K) and, as expected, the co-conformational equilibrium constant (k_2/k_{-2} = 0.6) favors the population of station I. From the fitting of the concentration-time traces upon addition of an excess of **2** (6 equivalents) to *Z*-**1**, the rate constants of the reactions in the lower half the network (Figure 2a) were obtained (Supporting Information, sections 6.2 and 6.3). The change in the co-conformational equilibrium constant of the *Z*-isomer (k_5/k_{-5} = 1.1) confirms that upon isomerization the macrocycle at station I is destabilized. The experiments also show that, at equilibrium, station II is more populated than *Z*-I, thus validating the order $K_{E\text{-I}} > K_{II} \gtrsim K_{Z\text{-I}}$. We assume that the rate constants for threading-dethreading of a second macrocycle, both before (k_3 and k_{-3}) and after (k_6 and k_{-6}) irradiation, have the same values as those for the first threading-dethreading.

2.4 | Experimental Demonstration of Pumping

The data gathered so far indicate that the system fulfils the two requirements to accomplish the directionally preferred transfer of the macrocycle along the axle by an energy ratchet mechanism upon *E*→*Z* photoisomerization, namely (i) the decrease of the complex stability at station I ($K_{E\text{-I}} > K_{Z\text{-I}}$), and (ii) the increase of the kinetic barrier on the azobenzene extremity that determines the directionality of the process. The question is now to assess whether the pump can operate autonomously under continuous irradiation in a dissipative non-equilibrium regime. In general, in dissipative states the concentrations of the species involved differ from their equilibrium values as long as energy is provided; once the input is stopped, the system returns to the closest energy minimum [34]. In the present system, light irradiation should deplete free **2** to generate a higher concentration of complexed species, that is, rings are pumped from solution and stored onto the axle. When light is switched off, part of the stored macrocycles should be released, while the system first relaxes to a kinetic trap (*Z*-azobenzenes species) and then evolves to the global equilibrium (*E*-isomer) upon slow thermal back isomerization.

Dissipative operation was observed by coupling time-resolved NMR spectroscopy with in situ sample irradiation to continuously monitor the concentration change of the species when the light source is turned on and off. In a typical experiment, equimolar amounts of *E*-**1** and **2** (~10 mM) were allowed to equilibrate in the dark at room temperature for 15 min. The mixture was successively irradiated until a stationary composition of the system was reached; at that point, light was switched off and data acquisition continued [52]. Given the complexity of the ^{1}H NMR spectra, the possibility to exploit ^{19}F signals, allowed by the trifluoromethyl label of **2**, was crucial for observing the time dependent evolution of the system, particularly with regard to the concentration of the free ring. Irradiation of the equilibrated mixture at λ = 369 ± 15 nm (Figure 4ab, yellow background)

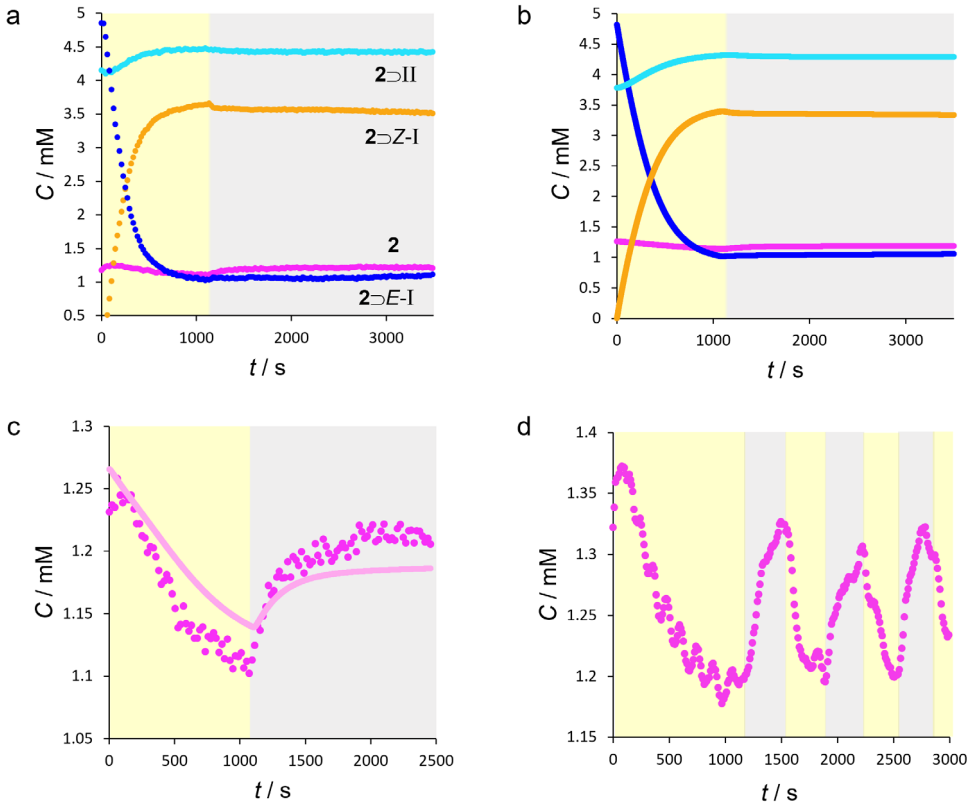

FIGURE 4 | (a) Concentration-time traces extracted from an array of ^{19}F NMR spectra (470 MHz, 298 K) recorded on a mixture of *E*-**1** (10.1 mM) and **2** (10.2 mM) in CD_3CN/CD_2Cl_2 7:3 upon irradiation (yellow background) and in the dark (grey background). The spectra were recorded at intervals of 20 s, and irradiation was performed with light of $\lambda = 369 \pm 15$ nm at an estimated photon flow of 4.65×10^{-8} Einstein s^{-1}. About 300 s of irradiation were required to reach an *E*/*Z* photostationary state. (b) Simulated concentration profiles corresponding to the experimental conditions adopted in a. (c) Magnified view of the concentration profile of the free macrocycle **2** (experimental: magenta dots; simulated: pink line). (d) Concentration changes of free **2** extracted from an array of ^{19}F NMR spectra (470 MHz, 298 K) recorded on a mixture of *E*-**1** (9.8 mM) and **2** (11 mM) in CD_3CN/CD_2Cl_2 7:3. The spectra were recorded at intervals of 10 s in a fatigue resistance test performed by alternating irradiation (300 s) and dark (300 s) periods. Irradiation was performed with light of $\lambda = 369 \pm 15$ nm at an estimated photon flow of 8.46×10^{-8} Einstein s^{-1}. The meaning of colors and labels is described in the caption of Figure 3.

causes the conversion of *E*-I⊂**2** (blue) into *Z*-I⊂**2** (orange); in consequence of the decrease of binding affinity of the pumping station ($K_{Z\text{-I}} < K_{E\text{-I}}$) and the inversion of the kinetic barriers ($k_{-4} << k_5$), complexed rings are transferred to station II instead of being released in solution, thus increasing the concentration of the species whose receiving station is encircled by a macrocycle (II⊂**2**, cyan). Significantly, exposure to light causes a decrease of the concentration of free **2** (Figure 4c, yellow background, magenta), mirrored by an increase of the overall concentration of complexed species ([2] and [3] pseudorotaxanes, Figure S61). As irradiation triggers both *E*→*Z* and *Z*→*E* isomerizations, re-opening the azobenzene "gate" in the species where the ring encircles station II—for example, *Z*-**1**⊂**2**^{II}→*E*-**1**⊂**2**^{II}—allows a second macrocycle to be loaded onto the axle ($t_{1/2} \cong 5$ s) before the first one can return to the pumping station ($t_{1/2} \cong 130$ s). Under constant irradiation, 5×10^{-8} mol (~ 0.1 mM) of **2** is loaded onto the axle, corresponding to about 8% of the uncomplexed macrocycles available in solution in the dark. Such a decrease of free rings is clearly a consequence of the dissipative non-equilibrium pumping because (i) the *E*/*Z* PSS is established on a faster time scale (about 300 s after the start of the irradiation), and (ii) the overall thermodynamic affinity of the axle for the ring is diminished by irradiation.

Upon switching the light off, a fraction of the accumulated macrocycles is released in solution (Figure 4c, grey background, magenta). Since rings can only escape from the azobenzene side of the axle and the dethreading rate is consistent with that of the *E*-isomer, it can be concluded that the increase of free macrocycle arises from partial dissociation of pseudorotaxanes *E*-**1**⊂**2**^{I} and *E*-**1**⊂(**2**)$_2$ present at PSS. A slight decrease of the *Z*-I⊂**2** species (Figure 4a, orange) and an increase of *E*-I⊂**2** (blue) are also observed, while II⊂**2** is practically unchanged (cyan). The interpretation of the complexes evolution is not as straightforward as for free **2**, because the experimental profiles result from the combination of multiple species. Since an effect of thermal *Z*→*E* isomerization can be excluded ($t_{1/2} \cong 130$ h at 298 K), these changes may be rationalized by considering a redistribution of rings between the two stations in the [2]pseudorotaxanes, namely, *E*-**1**⊂**2**^{II}→*E*-**1**⊂**2**^{I} and *Z*-**1**⊂**2**^{I}→*Z*-**1**⊂**2**^{II} [53]. The observed profiles are consistently reproduced by the mechanistic simulations (Figures 4b and S63). Alternated irradiation and dark cycles (Figures 4d and S62) demonstrated the stability of the system and the reproducibility of the phenomena.

In summary, our data show unambiguously that continuous irradiation drives the system to a dissipative non-equilibrium

state in which macrocycles are collected from solution to increase the population of the [3]pseudorotaxanes Z-**1**⊂(**2**)$_2$ and E-**1**⊂(**2**)$_2$. When the energy supply is interrupted, ring shuttling and dethreading adapt the concentrations to the previously photogenerated E/Z distribution, and the system is kinetically trapped until the stable E-isomers are thermally regenerated. Dissipative pumping can be resumed by turning the light on again.

2.5 | Numerical Simulations and Energetic Considerations

The determination of all the (photo)kinetic and spectroscopic parameters associated with the reaction network allowed us to perform numerical simulations of the concentration time profiles. The simulations rely on some reasonable assumptions (Supporting Information, section 8); nevertheless, they are consistent with the experimental data, corroborating the hypothesized mechanism and proving to be instrumental in rationalizing the processes underlying the experimental observations. The simulations reveal that the release of rings in the successive dark phase is not simply related to the disassembly of E-**1**⊂(**2**)$_2$. Actually, the non-equilibrium population of Z-**1**⊂**2**^{I} is converted into Z-**1**⊂**2**^{II} by ring shuttling; the enhanced complexation of station II is balanced out by the disappearance of E-**1**⊂**2**^{II} that becomes E-**1**⊂**2**^{I}, from which **2** could be released (Figure S64). An intriguing effect observed both experimentally and in simulations (Figure S63) is that, at the beginning of the irradiation, the system undergoes a transient regime in which a small amount of complexed macrocycles is released before the actual pumping starts. The phenomenon can be explained considering that, at the irradiation wavelength, the molar absorption coefficient of E-**1** is slightly larger when it is free than when it is complexed (Table S4). Therefore, $E \rightarrow Z$ photoisomerization is somewhat more efficient for the free axle, causing dethreading of the E-complexes by mass action. In the present case, such an information ratchet component counteracts the energy ratchet and lowers pumping efficiency; future studies could; however, explore how such effects might be used to improve device performance.

Considering that in a typical irradiation experiment ($\lambda = 369 \pm 15$ nm, $q = 4.65 \times 10^{-8}$ mol s^{-1}, 1100 s) the axle absorbs 4.5×10^{-5} mol of photons (Equation S20) and collects 5×10^{-8} mol of macrocycles, we can conclude that 900 photons are used, on average, to pump one ring. Under these conditions, the calculated energy density stored in the non-equilibrium steady state is 0.012 J L^{-1} (Equation S22) [11]. The efficiency of light-to-chemical energy transduction can be estimated when the system reaches a stationary condition and the energy absorbed from light is only used to sustain the non-equilibrium steady state [17, 51]. Based on the values calculated for the power dissipated by the complexation reactions and the absorbed light power, the energy conversion efficiency of the molecular pump in the conditions employed is about 0.9%. Such a low value mainly reflects the fact that most of the energy harvested from radiation is dissipated by the photoisomerization steps. It is interesting to note that, although our pump is fundamentally different from natural photosynthetic systems, it shares some common traits, such as the ability to process large amounts of light energy with high turnover, modest energy conversion efficiency, and minimal photodamage [24, 40].

3 | Conclusion

We have designed, synthesized and operated an artificial molecular pump capable of exploiting light energy to collect macrocycles from a solution and store them intramolecularly in a high-energy state. We demonstrated that the pump relies on energy ratcheting to directionally transfer macrocycles onto the collecting compartment, persisting in a dissipative non-equilibrium state sustained by light. Albeit with low efficiency, the energy of photons is converted into chemical potential: this represents a significant advance compared with previous systems, in which the contribution of repeated directional molecular movements could not be harvested and stored. These results highlight the potential of the (supra)molecular bottom-up approach for the construction of functional photoactive nanostructures and provide a foundation for the development of useful molecular-based light-controlled devices and materials. Future efforts will be directed toward improving pumping efficiency, enhancing energy storage capability, and integrating such systems into more complex functional architectures.

Acknowledgments

This work was supported by the European Union through the European Research Council, Advanced (AdG no.692981 to A. C.).

Open access publishing facilitated by Universita di Bologna, as part of the Wiley - CRUI-CARE agreement.

Conflicts of Interest

The authors declare no conflicts of interest.

Data Availability Statement

The data that supports the findings of this study are available in the supplementary material of this article

References

1. D. S. Goodsell, *The Machinery of Life*, *second edition* (Copernicus, 2009), https://doi.org/10.1007/978-0-387-84925-6.

2. P. M. Hoffman, *Life's Ratchet. How Molecular Machines Extract Order From Chaos* (Basic Books, 2012).

3. D. C. Gadsby, "Ion Channels Versus Ion Pumps: The Principal Difference, in Principle," *Nature Reviews Molecular Cell Biology* 10 (2009): 344–352, https://doi.org/10.1038/nrm2668.

4. V. Balzani, A. Credi, F. M. Raymo, and J. F. Stoddart, "Artificial Molecular Machines," *Angewandte Chemie International Edition* 39 (2000): 3348–3391, https://doi.org/10.1002/1521-3773(20001002)39:19⟨3348::AID-ANIE3348⟩3.0.CO;2-X.

5. S. Kassem, A. T. L. Lee, D. A. Leigh, A. Markevicius, and J. Solà, "Pick-Up, Transport and Release of a Molecular Cargo Using a Small-Molecule Robotic Arm," *Nature Chemistry* 8 (2016): 138–143, https://doi.org/10.1038/nchem.2410.

6. C. Schäfer, G. Ragazzon, B. Colasson, M. La Rosa, S. Silvi, and A. Credi, "An Artificial Molecular Transporter," *ChemistryOpen* 5 (2016): 120–124, https://doi.org/10.1002/open.201500217.

7. T. J. Johnson and M. J. Langton, "Molecular Machines for the Control of Transmembrane Transport," *Journal of the American Chemical Society* 145 (2023): 27167–27184, https://doi.org/10.1021/jacs.3c08877.

8. S. Chen, Y. Wang, T. Nie, et al., "An Artificial Molecular Shuttle Operates in Lipid Bilayers for Ion Transport," *Journal of the American Chemical Society* 140 (2018): 17992–17998, https://doi.org/10.1021/jacs.8b09580.

9. A. Credi, "A Molecular Cable Car for Transmembrane Ion Transport," *Angewandte Chemie International Edition* 58 (2019): 4108–4110, https://doi.org/10.1002/anie.201814333.

10. M. N. Chatterjee, E. R. Kay, and D. A. Leigh, "Beyond Switches: Ratcheting a Particle Energetically Uphill With a Compartmentalized Molecular Machine," *Journal of the American Chemical Society* 128 (2006): 4058–4073, https://doi.org/10.1021/ja057664z.

11. V. Serreli, C.-F. Lee, E. R. Kay, and D. A. Leigh, "A Molecular Information Ratchet," *Nature* 445 (2007): 523–527, https://doi.org/10.1038/nature05452.

12. C. Cheng, P. R. McGonigal, W.-G. Liu, et al., "Energetically Demanding Transport in a Supramolecular Assembly," *Journal of the American Chemical Society* 136 (2014): 14702–14705, https://doi.org/10.1021/ja508615f.

13. K. Liang, F. Nicoli, S. Al Shehimy, et al., "Catalysis-Driven Active Transport Across a Liquid Membrane," *Angewandte Chemie International Edition* 64 (2025): e202421234, https://doi.org/10.1002/anie.202421234.

14. "Special Issue: Molecular Motors" *Chem. Rev*. **2020**, 120, 1–460.

15. M. A. Watson and S. L. Cockroft, "Man-Made Molecular Machines: Membrane Bound," *Chemical Society Reviews* 45 (2016): 6118–6129, https://doi.org/10.1039/C5CS00874C.

16. R. D. Astumian, C. Pezzato, Y. Feng, et al., "Non-Equilibrium Kinetics and Trajectory Thermodynamics of Synthetic Molecular Pumps," *Materials Chemistry Frontiers* 4 (2020): 1304–1314, https://doi.org/10.1039/D0QM00022A.

17. T. Sangchai, S. Al Shehimy, E. Penocchio, and G. Ragazzon, "Artificial Molecular Ratchets: Tools Enabling Endergonic Processes," *Angewandte Chemie International Edition* 62 (2023): e20230950.

18. S. Borsley, D. A. Leigh, and B. M. W. Roberts, "Molecular Ratchets and Kinetic Asymmetry: Giving Chemistry Direction," *Angewandte Chemie International Edition* 63 (2024): e202400495, https://doi.org/10.1002/anie.202400495.

19. Y. Qiu, Y. Feng, Q.-H. Guo, R. D. Astumian, and J. F. Stoddart, "Pumps Through The Ages," *Chem* 6 (2020): 1952.

20. C. Cheng, P. R. McGonigal, S. T. Schneebeli, et al., "An Artificial Molecular Pump," *Nature Nanotechnology* 10 (2015): 547–553, https://doi.org/10.1038/nnano.2015.96.

21. S. Amano, S. D. P. Fielden, and D. A. Leigh, "A Catalysis-Driven Artificial Molecular Pump," *Nature* 594 (2021): 529–534, https://doi.org/10.1038/s41586-021-03575-3.

22. C. Pezzato, M. T. Nguyen, D. J. Kim, O. Anamimoghadam, L. Mosca, and J. F. Stoddart, "Controlling Dual Molecular Pumps Electrochemically," *Angewandte Chemie International Edition* 57 (2018): 9325–9329, https://doi.org/10.1002/anie.201803848.

23. M. Baroncini, J. Groppi, S. Corra, S. Silvi, and A. Credi, "Light-Responsive (Supra)Molecular Architectures: Recent Advances," *Advanced Optical Materials* 7 (2019): 1900392, https://doi.org/10.1002/adom.201900392.

24. L. O. Björn, ed., *Photobiology—The Science of Life and Light* (Springer, 2008).

25. M. Wikström, ed., *Mechanisms of Primary Energy Transduction in Biology* (RSC Publishing, 2018).

26. G. Steinberg-Yfrach, J.-L. Rigaud, E. N. Durantini, A. L. Moore, D. Gust, and T. A. Moore, "Light-Driven Production of ATP Catalysed by F0F1-ATP Synthase in an Artificial Photosynthetic Membrane," *Nature* 392 (1998): 479–482, https://doi.org/10.1038/33116.

27. I. M. Bennett, H. M. V. Farfano, F. Bogani, et al., "Active Transport of Ca^{2+} by an Artificial Photosynthetic Membrane," *Nature* 420 (2002): 398–401, https://doi.org/10.1038/nature01209.

28. "Photochemistry of Supramolecular Systems and Nanostructured Assemblies. In memory of Professor Nick Turro (1938–2012)" *Chemical Society Reviews* 43 (2014): 4003, https://doi.org/10.1039/c4cs90032d.

29. N. Koumura, R. W. J. Zijlstra, R. A. van Delden, N. Harada, and B. L. Feringa, "Light-Driven Monodirectional Molecular Rotor," *Nature* 401 (1999): 152–155, https://doi.org/10.1038/43646.

30. L. Greb, A. Eichhöfer, and J.-M. Lehn, "Synthetic Molecular Motors: Thermal N Inversion and Directional Photoinduced C═N Bond Rotation of Camphorquinone Imines," *Angewandte Chemie International Edition* 54 (2015): 14345–14348, https://doi.org/10.1002/anie.201506691.

31. A. Gerwien, P. Mayer, and H. Dube, "Green Light Powered Molecular State Motor Enabling Eight-Shaped Unidirectional Rotation," *Nature Communications* 10 (2019): 4449, https://doi.org/10.1038/s41467-019-12463-4.

32. D. R. S. Pooler, A. S. Lubbe, S. Crespi, and B. L. Feringa, "Designing Light-Driven Rotary Molecular Motors," *Chemical Science* 12 (2021): 14964–14986, https://doi.org/10.1039/D1SC04781G.

33. S. Corra, M. Curcio, and A. Credi, "Photoactivated Artificial Molecular Motors," *Journal of the American Chemical Society Au* 3 (2023): 1301–1313, https://doi.org/10.1021/jacsau.3c00089.

34. M. Kathan and S. Hecht, "Photoswitchable Molecules as Key Ingredients to Drive Systems away From the Global Thermodynamic Minimum," *Chemical Society Reviews* 46 (2017): 5536–5550, https://doi.org/10.1039/C7CS00112F.

35. M. Weissenfels, J. Gemen, and R. Klajn, "Dissipative Self-Assembly: Fueling With Chemicals Versus Light," *Chemistry* 7 (2021): 23–37, https://doi.org/10.1016/j.chempr.2020.11.025.

36. D. Daou, Y. Zarate, M. Maaloum, et al., "Out-of-Equilibrium Mechanical Disruption of β-Amyloid-Like Fibers Using Light-Driven Molecular Motors," *Advanced Materials* 36 (2024): 2311293, https://doi.org/10.1002/adma.202311293.

37. B. Sachini, S. Corra, M. Curcio, J. Groppi, and A. Credi, "Defying Chemical Equilibrium With Light," *Trends in Chemistry* 7 (2025): 372–383, https://doi.org/10.1016/j.trechm.2025.04.009.

38. T. Wachsmuth, R. Kluifhooft, M. Müller, L. Zeiss, and M. Kathan, "A Molecular Machine Directs the Synthesis of a Catenane," *Science* 389 (2025): 526–531, https://doi.org/10.1126/science.adx5363.

39. R. Kluifhooft, T. Wachsmuth, B. Barthel, M. Müller, A.-K. Rückert, and M. Kathan, "A Molecular Machine Directs the Synthesis of a Rotaxane," *Angewandte Chemie International Edition* 65 (2026): e20085, https://doi.org/10.1002/anie.202520085.

40. D. K. Dogutan and D. G. Nocera, "Artificial Photosynthesis at Efficiencies Greatly Exceeding That of Natural Photosynthesis," *Accounts of Chemical Research* 52 (2019): 3143–3148, https://doi.org/10.1021/acs.accounts.9b00380.

41. A. Arduini, R. Bussolati, A. Credi, et al., "Towards Controlling the Threading Direction of a Calix[6]arene Wheel by Using Nonsymmetric Axles," *Chemistry – A European Journal* 15 (2009): 3230–3242, https://doi.org/10.1002/chem.200801926.

42. M. Baroncini, S. Silvi, M. Venturi, and A. Credi, "Photoactivated Directionally Controlled Transit of a Non-Symmetric Molecular Axle Through a Macrocycle," *Angewandte Chemie International Edition* 51 (2012): 4223–4226, https://doi.org/10.1002/anie.201200555.

43. N. N. Bach, V. Josef, H. Maid, and H. Dube, "Active Mechanical Threading by a Molecular Motor**," *Angewandte Chemie International Edition* 61 (2022): e202201882, https://doi.org/10.1002/anie.202201882.

44. B. Shao, H. Fu, and I. Aprahamian, "A Molecular Anion Pump," *Science* 385 (2024): 544–549, https://doi.org/10.1126/science.adp3506.

45. J. Pruchyathamkorn, B.-N. T. Nguyen, A. B. Grommet, et al., "Harnessing Maxwell's Demon to Establish a Macroscale Concentration Gradient," *Nature Chemistry* 16 (2024): 1558–1564, https://doi.org/10.1038/s41557-024-01549-2.

46. G. Ragazzon, M. Baroncini, S. Silvi, M. Venturi, and A. Credi, "Light-Powered Autonomous and Directional Molecular Motion of a Dissipative Self-Assembling System," *Nature Nanotechnology* 10 (2015): 70–75, https://doi.org/10.1038/nnano.2014.260.

47. J. Groppi, L. Casimiro, M. Canton, et al., "Precision Molecular Threading/Dethreading," *Angewandte Chemie International Edition* 59 (2020): 14825–14834, https://doi.org/10.1002/anie.202003064.

48. S. Corra, L. Casimiro, M. Baroncini, et al., "Artificial Supramolecular Pumps Powered by Light," *Chemistry European Journal* 27 (2021): 11076–11083, https://doi.org/10.1002/chem.202101163.

49. M. Canton, J. Groppi, L. Casimiro, et al., "Second-Generation Light-Fueled Supramolecular Pump," *Journal of the American Chemical Society* 143 (2021): 10890–10894, https://doi.org/10.1021/jacs.1c06027.

50. A. Sabatino, E. Penocchio, G. Ragazzon, A. Credi, and D. Frezzato, "Individual-Molecule Perspective Analysis of Chemical Reaction Networks: The Case of a Light-Driven Supramolecular Pump," *Angewandte Chemie International Edition* 58 (2019): 14341–14348, https://doi.org/10.1002/anie.201908026.

51. S. Corra, M. Tranfić Bakić, J. Groppi, et al., "Kinetic and Energetic Insights Into the Dissipative Non-Equilibrium Operation of an Autonomous Light-Powered Supramolecular Pump," *Nature Nanotechnology* 17 (2022): 746–751, https://doi.org/10.1038/s41565-022-01151-y.

52. *Irradiation* experiments were performed With either nearly monochromatic light (λ = 365 ± 5 nm) or broadband light (λ = 369 ± 15 nm) and monitored by both ^{1}H NMR and ^{19}F NMR (Supporting Information, section 7).

53. An increase of *E*-**1**⊂**2**^{I} by re-threading of *E*-**1** into **2** is not consistent with the observed increase of free **2**, whereas a depletion of *Z*-**1**⊂**2**^{I} by dethreading (k_{-4}) would be far too slow on the observed time scale.

54. M. Curcio, F. Nicoli, E. Paltrinieri, et al., "Chemically Induced Mismatch of Rings and Stations in [3]Rotaxanes," *Journal of the American Chemical Society* 143 (2021): 8046–8055, https://doi.org/10.1021/jacs.1c02230.

55. S. J. Cantrill, G. J. Youn, J. F. Stoddart, and D. J. Williams, "Supramolecular Daisy Chains," *Journal of Organic Chemistry* 66 (2001): 6857–6872, https://doi.org/10.1021/jo010405h.

56. F. V. Marcoline, J. Furth, S. Nayak, M. Grabe, and R. I. Macey, "Berkeley Madonna Version 10-A Simulation Package for Solving Mathematical Models," *CPT: PSP* 11 (2022): 290.

57. M. Montalti, A. Credi, L. Prodi, and M. T. Gandolfi, *Handbook of Photochemistry*, 3rd ed. (CRC Press, 2006), https://doi.org/10.1201/9781420015195.

58. E. Fischer, "Calculation of Photostationary States in Systems A .Dblarw. B When Only A is Known," *Journal of Physical Chemistry* 71 (1967): 3704–3706, https://doi.org/10.1021/j100870a063.

59. L. Casimiro, L. Andreoni, J. Groppi, A. Credi, R. Métivier, and S. Silvi, "4,4′-Dimethylazobenzene as a Chemical Actinometer," *Photochemical & Photobiological Sciences* 21 (2022): 825–833, https://doi.org/10.1007/s43630-021-00162-3.

60. A. Arduini, R. Bussolati, A. Credi, et al., "Toward Directionally Controlled Molecular Motions and Kinetic Intra- and Intermolecular Self-Sorting: Threading Processes of Nonsymmetric Wheel and Axle Components," *Journal of the American Chemical Society* 135 (2013): 9924–9930, https://doi.org/10.1021/ja404270c.

Supporting Information

Additional supporting information can be found online in the Supporting Information section.

The authors have cited additional references within the Supporting Information [54–60].

Supporting File: anie72137-sup-0001-SuppMat.pdf.